ACS APPLIED MATERIALS & INTERFACES

www.acsami.org

Research Article

Achieving Low Voltage Plasma Discharge in Aqueous Solution Using Lithographically Defined Electrodes and Metal/Dielectric Nanoparticles

Ruoxi Li, Indu Aravind, Sizhe Weng, Zhi Cai, Boxin Zhang, and Stephen B. Cronin*

Cite This: *ACS Appl. Mater. Interfaces* 2024, 16, 33571−33577

Read Online

ACCESS | Metrics & More | Article Recommendations | Supporting Information

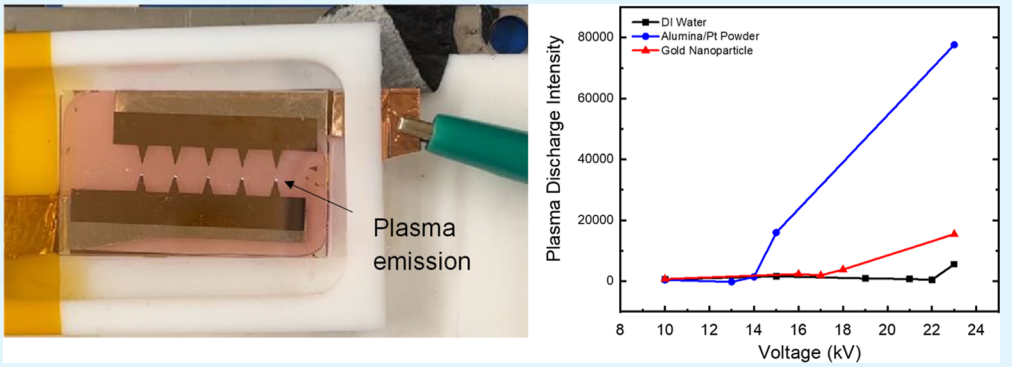

ABSTRACT: Because of the high dielectric strength of water, it is extremely difficult to discharge plasma in a controllable way in the aqueous phase. By using lithographically defined electrodes and metal/dielectric nanoparticles, we create electric field enhancement that enables plasma discharge in liquid electrolytes at significantly reduced applied voltages. Here, we use high voltage (10−30 kV) nanosecond pulse (20 ns) discharges to generate a transient plasma in the aqueous phase. An electrode geometry with a radius of curvature of approximately 10 μm, a gap distance of 300 μm, and an estimated field strength of 5×10^6 V/cm resulted in a reduction in the plasma discharge threshold from 28 to 23 kV. A second structure had a radius of curvature of around 5 μm and a gap distance of 100 μm had an estimated field strength of 9×10^6 V/cm but did not perform as well as the larger gap electrodes. Adding gold nanoparticles (20 nm diameter) in solution further reduced the threshold for plasma discharge to 17 kV due to the electric field enhancement at the water/gold interface, with an estimated *E*-field enhancement of 4×. Adding alumina nanoparticles decorated with Pt reduced the plasma discharge threshold to 14 kV. In this scenario, the emergence of a triple point at the juncture of alumina, Pt, and water results in the coexistence of three distinct dielectric constants at a singular location. This leads to a notable concentration of electric field, effectively aiding in the initiation of plasma discharge at a reduced voltage. To gain a more comprehensive and detailed understanding of the electric field enhancement mechanism, we performed rigorous numerical simulations. These simulations provide valuable insights into the intricate interplay between the lithographically defined electrodes, the nanoparticles, and the resulting electric field distribution, enabling us to extract crucial information and optimize the design parameters for enhanced performance.

KEYWORDS: *plasma discharge, aqueous solution, nanoparticle, electric field, photolithography*

1. INTRODUCTION

The application of plasma technology in various research fields like clean fuel generation, pollutant conversion, and wastewater treatment is discussed, showcasing its potential for future catalytic applications.[1−6] In addition, plasma-catalyst hybrid systems can advance efficient CO_2 conversion processes, and plasma generation techniques can be developed in sustainable energy applications.[7] However, a vast majority of previous literature on plasma-driven chemistry has been limited to gas-phase reactions.[8] The main reason for this is that it is extremely difficult to discharge plasma in a controllable way in the aqueous phase due to the high dielectric strength of water. The mechanism behind the initiation of plasma discharge in liquid is thought to be through the generation of nanopores. Previous research from Zhang et al. investigated the influence of the material dielectric constant on plasma generation inside catalyst

Received: April 12, 2024
Revised: June 6, 2024
Accepted: June 10, 2024
Published: June 20, 2024

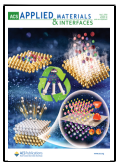

pores, revealing that lower dielectric constants enhance ionization inside the pore, while higher dielectric constants lead to increased ionization in the sheath, providing valuable insights for optimizing plasma catalysis processes, and found that different pore sizes influence plasma generation.[9] These elongated ellipsoidal voids, in the direction of the electric field, are due to a strong inhomogeneous electric field rearrangement of the elementary dipoles on a time scale much shorter than the counteracting hydrodynamic flow.[10,11] The rise time of the high voltage pulse ($dV/dt = 10^{12}$ V/s) must be short enough to produce the negative pressure zones, while being long enough to allow them to grow to the critical size.[12,13] Once the nanopore reaches this size, a primary liquid phase streamer, which is a common initial stage of electrical discharge that forms from the electrons within the nanopore, experiences an acceleration from the electric field that surpasses the ionization energy of water molecules.[14,15] After the electrons reach the electrode, the liquid's positive ions form a new electrode, and the process cascades.[10] This electrostriction creation of nanovoids from rapidly pulsed high voltages has been experimentally supported through various studies.[11,13,16] As such, this plasma initiation mechanism is unique to the fast rise times of the nanosecond pulse discharges.

Yang et al. recently demonstrated plasma discharge in CO_2 saturated water, which drives the reduction of CO_2 to higher order hydrocarbons (including acetate $C_2H_3O_2^-$, formic acid CH_2O_2, acetic acid CH_3COOH, and format HCO_2^-).[17] This process involves the generation of neutral species and radicals and then recombination to form new chemical processes that can be observed through nuclear magnetic resonance spectroscopy and liquid ion chromatography. One application of plasma chemistry is the production of stable oxidizers, such as plasma acid, that can be used across many applications, from food sterilization to industrial cleaning. Plasma acid contains superoxide anions O_2^- and hydrogen cations H^+ and is generated from plasma discharge in pure deionized water. While other groups have explored plasma formed with discharge above the liquid surface,[18,19] the work presented here initiates the plasma discharge directly within the solution.

2. MATERIALS AND METHODS

As mentioned above, generating a plasma discharge in liquid water is a highly challenging task because of the high dielectric strength of water. Lithographically defined electrodes can create electric field enhancement, as shown in Figures 1 and 2. These stand in contrast to the electrodes used previously, which were prepared by hand using copper tape and a razor blade. Here, the tip radius is around 20 μm, as measured with an optical microscope.[17,20,21] In this study, electrodes were fabricated through a series of steps. Initially, electrodes were patterned using photolithography, followed by the deposition of Au via e-beam evaporation. The process began by spinning a layer of 1,1,1,3,3,3-hexaméthyldisilazane (HMDS, Cat# AC120580025 from Thermo Fisher Scientific) onto a glass substrate at 500 rpm for 5 s and 3500 rpm for 60 s, succeeded by the application of AZ5214 (#697316 from Merck KGaA) with same spinning speed, and subsequently baking it for 1 min at 110 °C. The pattern transfer onto the sample was achieved using an Aligner MJB3 under 100 mW dose power, followed by development using AZ 726 MIF developer from AZ electronic materials. Finally, a 100 nm gold film was deposited onto the sample using electron -beam evaporation before using acetone to lift off the photoresist overnight to obtain the final structure, as shown in Figure 1b. It is worth noting that, while both Au and Pd are commonly utilized materials for electrodes, Pd was not employed in this study due to its higher melting point. The higher power required during Pd evaporation could potentially overbake the photoresist, complicating the lift-off process. We also tried several other electrode materials for which details have been given in the Supporting Information document. By reducing the gap distance and using sharper electrode tips, we achieved higher electric fields (at a given voltage), resulting in more efficient plasma discharge.[17] Specifically, we defined two structures for our experiments: the first structure had a radius of curvature of approximately 10 μm, a gap distance of 300 μm, and an estimated field strength of 5×10^6 V/cm. The second structure had a radius of curvature of around 5 μm and a gap distance of 100 μm.

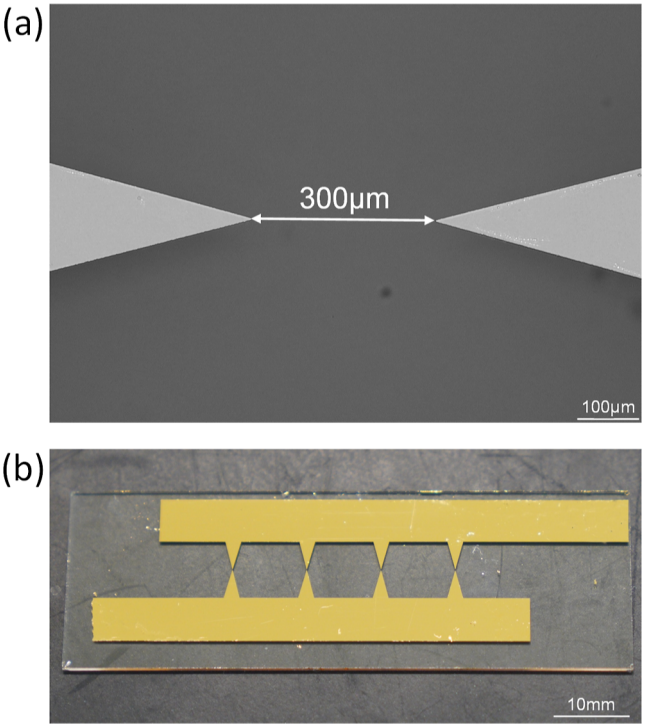

Figure 1. (a) Image of the lithographically defined electrode tips with a 300 μm gap size under an optical microscope. (b) Image of lithographically defined electrodes with smaller gaps (100 μm) on a 75 × 25 × 1 mm glass slide.

To estimate the electric field distribution around the tip of the lithographically defined electrodes, we perform static simulations using the electrostatic physics package in the AC/DC module available in the COMSOL Multiphysics solutions. The geometry used in the simulation is illustrated in Figure 2a. Here, triangular-shaped gold tips are simulated on top of a glass slide ($\varepsilon = 6.7$) in an aqueous dielectric ($\varepsilon = 78.6$). For the simulation shown in Figure 2b, a peak field of 3×10^7 V/cm is predicted under an applied voltage of 20 kV. The tip has a terminating curvature of $r_{tip} = 5$ μm and a gap size of 10 μm (gap = $2r_{tip}$). Figure 2c plots the calculated peak electric fields produced as a function of electrode gap with sizes ranging from 5 μm to 2 mm, all of which are well above the threshold for plasma discharge in aqueous solution. Here, we use a physics-optimized mesh for the system with tetrahedral meshes having a minimum mesh size of 0.3 μm and a maximum mesh size of 300 μm. The minimum feature size of our photolithography is approximately 1−2 μm. Therefore, we only explored tip radii of 1 μm and larger. We also explored gap sizes of 10, 30, 50, 70, 100, and 300 μm. Experimentally, however, we found that a gap size of 300 μm worked best for producing stable plasma, and smaller gaps tended to arc uncontrollably.

Figure 3a shows a schematic diagram of the experimental setup used for obtaining plasma emission intensity-time traces at the surface of our lithographically defined electrode surfaces under high voltage nanosecond pulse discharge. The setup uses a high voltage nanosecond pulse generator (Transient Plasma Systems Inc., model 30×), which produces up to 30 kV pulses, 20 ns in duration, as shown in Figure 3a. Figure 3b shows a cross-section schematic diagram of our

https://doi.org/10.1021/acsami.4c06007
ACS Appl. Mater. Interfaces 2024, 16, 33571−33577

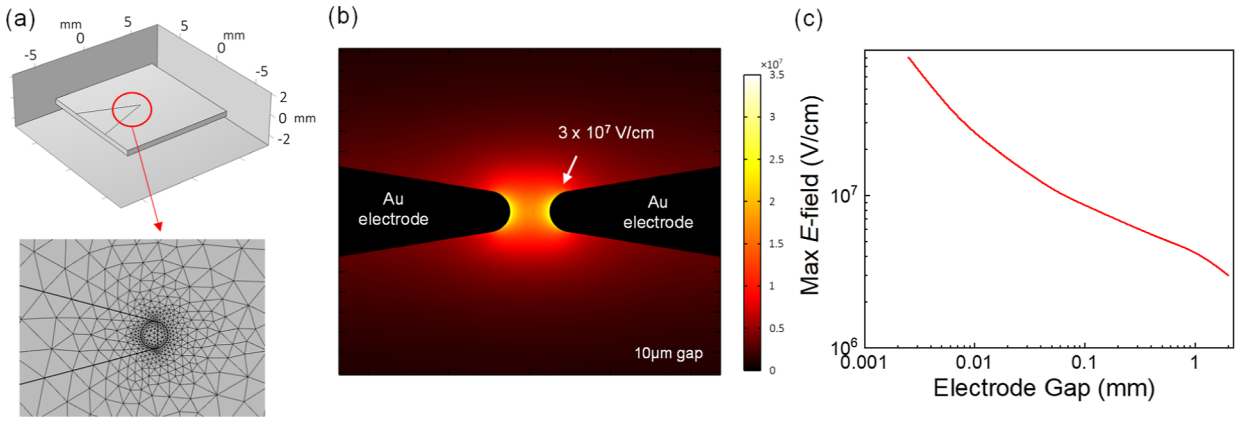

Figure 2. (a) Electric field simulations of various electrode geometries, showing a schematic diagram of the physics-optimized mesh with tetrahedral meshes having a minimum mesh size of 0.3 μm and maximum mesh size of 300 μm. (b) Plot of the electric field profile obtained across the top surface of the electrodes. (c) Maximum electric field plotted as a function of the electrode gap at 20 kV.

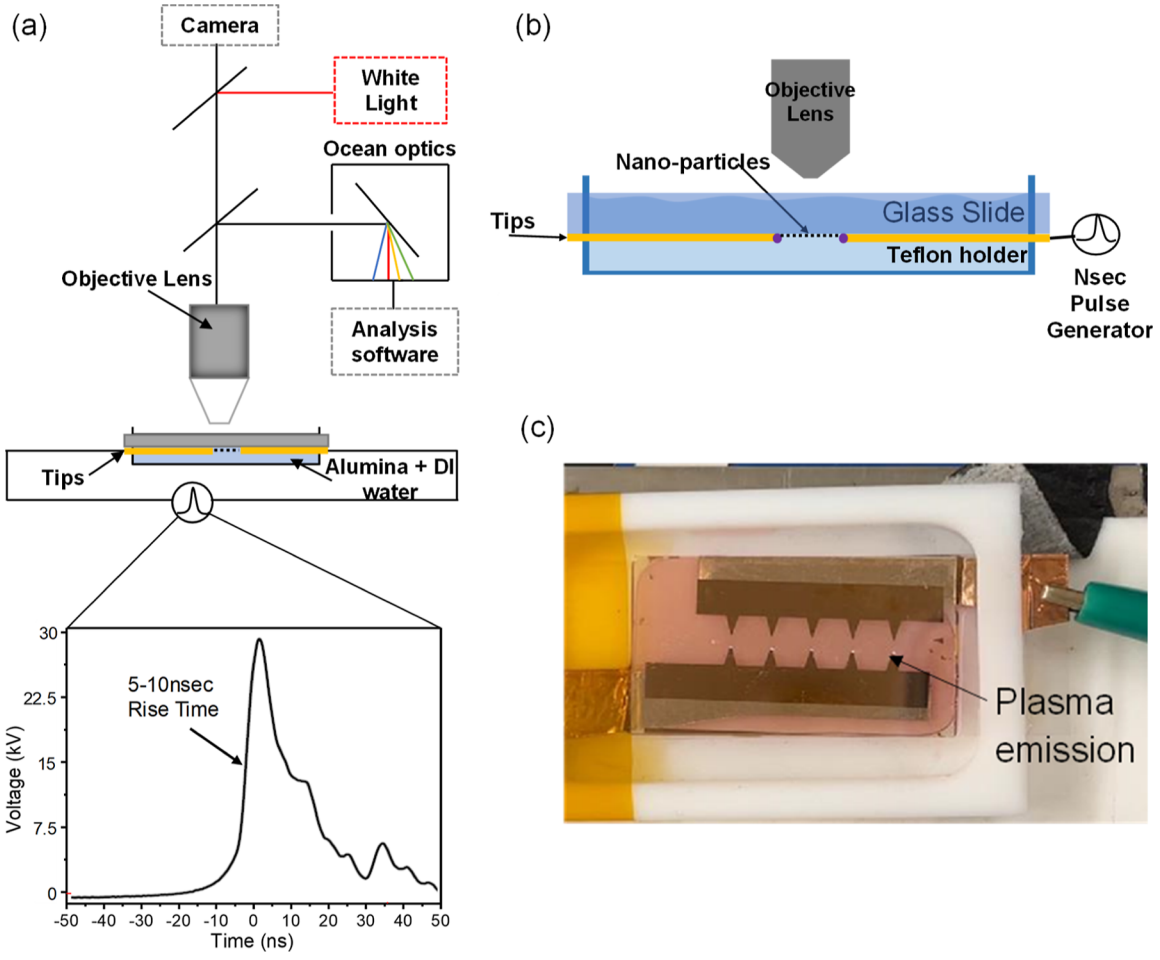

Figure 3. (a) Schematic diagram illustrating spectroscopy of electrode surfaces using a glass correction objective lens under high voltage nanosecond pulse discharge. (b) Cross-sectional diagram of the experimental setup used to obtain in situ plasma emission intensity-time traces. (c) Photograph of plasma emission using electrodes with a 300 μm gap distance.

experimental setup for observing plasma emission spectroscopy. Here, a gold lithographically defined electrode supported on glass, separated by a 300 μm gap, is immersed in an aqueous solution and held by a Teflon holder, while the top surface of the glass slide remains exposed to air. This "flipped" geometry enables plasma emission intensity-time traces to be taken efficiently using a glass-corrected objective lens (Olympus LUCPlanFLN 40×/0.6) that is carefully aligned with our spectrometer. The nanosecond pulse is used to apply high voltage, and plasma emission is generated between two tips, as shown in Figure 3c.

3. DISCUSSION

The process of plasma discharge in liquid is a stochastic process that occurs randomly within our relatively small focal volume, making it difficult to predict and measure. However, by

https://doi.org/10.1021/acsami.4c06007
ACS Appl. Mater. Interfaces 2024, 16, 33571−33577

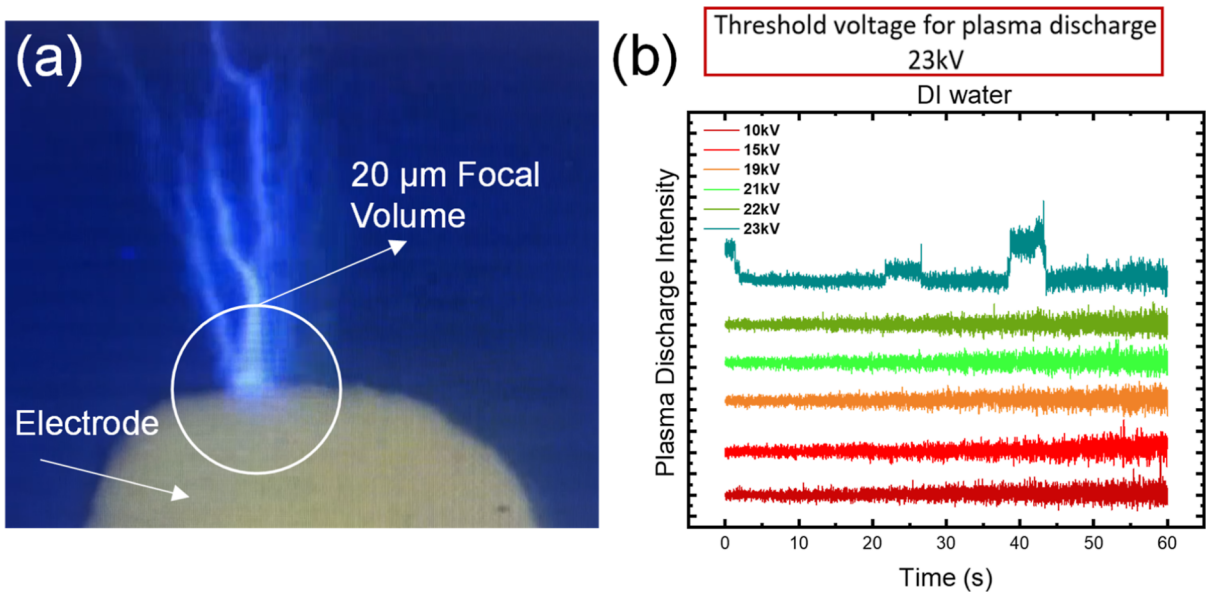

Figure 4. (a) Transient plasma emission observed under an optical microscope under high voltage nanosecond pulse discharges at 23 kV and (b) corresponding intensity-time traces showing plasma emission when the voltage is 23 kV.

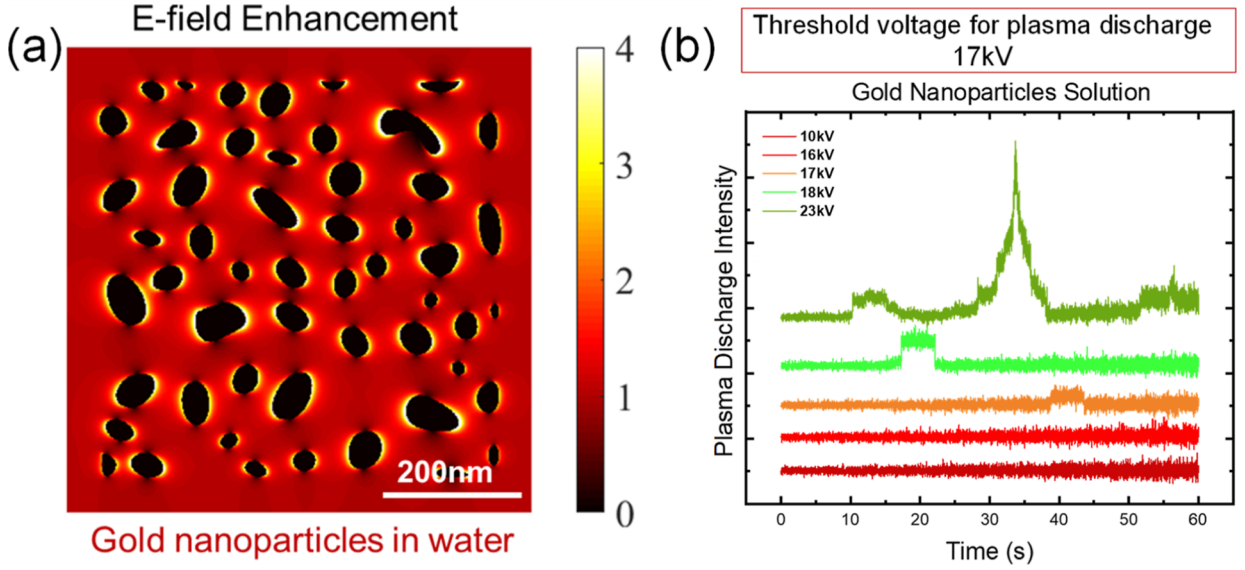

Figure 5. (a) Electric field strength calculated using numerical electrostatic simulations in gold nanoparticles in DI water. (b) Intensity-time traces generated with gold electrodes in gold nanoparticle solution at 16 kV.

analyzing the intensity-time traces produced during these discharges, we can determine the onset voltage for plasma discharge, which provides valuable insight into the process. Raw data and more details have been given in the Supporting Information document. Our research found that using lithographically defined electrodes significantly reduces the voltage needed to achieve plasma discharge in liquid. Our experiments showed that the threshold voltage for plasma discharge was around 23 kV (as shown in Figure 4), a significant reduction from the voltage required without the lithographic electrodes. Previously, we observed that when using copper tape, a voltage of 28 kV is required to initiate plasma discharge, but a discharge voltage of only 23 kV is required when using lithographic electrodes in deionized water (#7732-18-5 from VWR, with a resistivity of 18 MΩ·cm). Figure 4a shows plasma discharge in deionized (DI) water observed at 23 kV. In Figure 4b, the data appear as random telegraph noise, reflecting the stochastic nature of the plasma discharge process, which fits within our focal volume only occasionally.

We have also found that adding 20 nm diameter Au nanoparticles (Sigma-Aldrich #741965) can reduce the threshold voltage required for plasma discharge in DI water, as shown in Figure 5. Figure 5a shows the electric field strength produced with gold nanoparticles in DI water calculated using static simulations with the electrostatic physics package in COMSOL, which exhibits a 4× enhancement in the local strength. Here, the dielectric constants were taken as glass slide ($\varepsilon_o = 6.7$), aqueous dielectric ($\varepsilon_o = 78.6$), and gold (complex index of refraction: $n = 0.467 + 2.415i$). Figure 5b shows the plasma emission intensity plotted as a function of the peak pulse voltage. This demonstrates that the threshold voltage for plasma discharge in DI water can be reduced from 22 to 17 kV by adding metal

https://doi.org/10.1021/acsami.4c06007
ACS Appl. Mater. Interfaces 2024, 16, 33571−33577

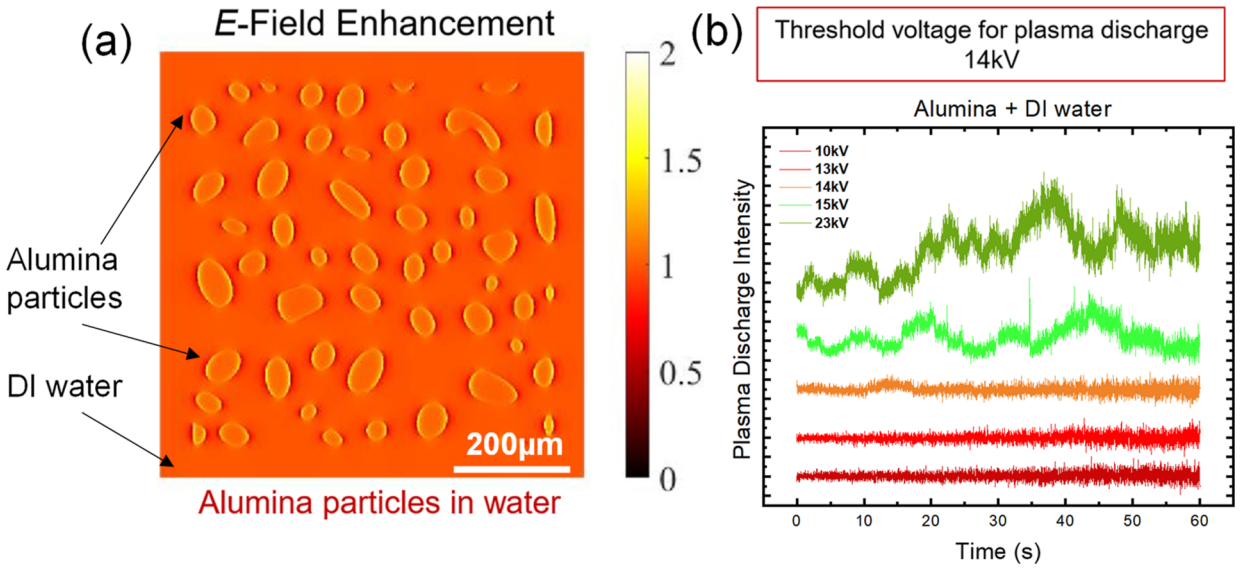

Figure 6. (a) Electron field strength calculated using numerical electrostatic simulations and (b) intensity-time traces obtained with different pulse voltage discharge in DI water with alumina nanoparticles decorated with Pt.

nanoparticles to the solution. While gold is rather catalytically inert, catalytic materials (e.g., Ir, Ru, and Ni) can be introduced to provide catalytically active sites for directing various reaction pathways toward desired products.

We have also discovered that adding Pt-loaded alumina nanoparticles, which are sized between 50 to 150 μm (Sigma-Aldrich #205974, 5 wt % loading, powder), can lower the voltage needed to start plasma discharge in DI water. One possible explanation for this effect is the formation of a triple point at the interface between the alumina nanoparticles, Pt, and water. This triple point creates a unique situation where three different dielectric constants are present at the same point, which is associated with a large electric field concentration that helps facilitate plasma discharge at a lower voltage. Figure 6a shows the results of electric field simulations, which show an enhancement of 2× at the Al_2O_3/water interface. This relatively small field enhancement can greatly affect plasma discharge thresholds, since the field emission of electrons depends exponentially on the electric field strength. Also, these simulations do not include the effects of the Pt nanoparticles. Figure 6b shows that the onset of plasma discharge occurs at 14 kV, nearly half of the required voltage needed without the alumina nanoparticles and lithographically defined electrodes. Additionally, the presence of Pt on the alumina nanoparticles provides a catalytically active surface that can assist in plasma-driven reactions, further enhancing the efficiency of the system. It should be noted that the oxygen radicals in the plasma (atomic O and O_3) tend to break down carbon-based molecules (e.g., ligands). Here, however, the Pt is not bound to the alumina by organic molecules. These findings suggest that adding Pt-loaded alumina nanoparticles could offer a promising approach toward achieving efficient and controllable plasma discharge in liquids, with potential applications in fields such as water treatment and renewable energy.

Figure 7 illustrates the relationship between plasma discharge intensity and nanosecond pulse voltage obtained in DI water, both with and without gold nanoparticles and alumina particles as intermedia. This plot shows that a significant enhancement is achieved by using the alumina particles than by the other two methods. Specifically, plasma can be initiated at voltages as low

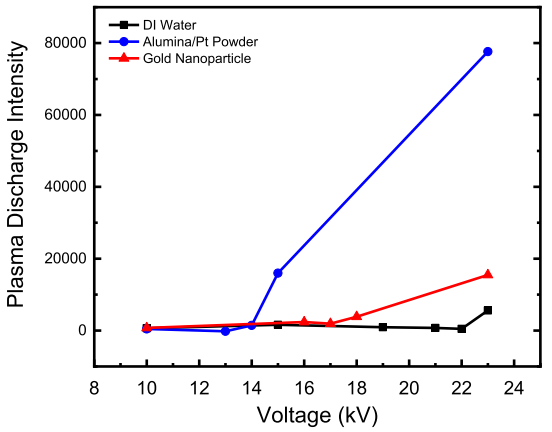

Figure 7. Plasma discharge intensity (luminescence intensity) generated in DI water with and without gold nanoparticles and alumina particles plotted as a function of nanosecond pulse voltage.

as 14 kV, corresponding to a significant reduction in energy consumption and reduced power supply cost. In addition, the plasma discharge intensity observed with alumina nanoparticles was 15× stronger than in DI water at a discharge voltage of 22 kV.

Achieving low-voltage plasma discharge in aqueous solutions opens new possibilities across various fields. In manufacturing, plasma-based technologies can enhance surface modification, cleaning, and sterilization, improving product quality and efficiency. In materials processing, reduced voltage plasma discharge allows for precision etching, thin film deposition, and surface functionalization, enabling high-performance components. Environmentally, this offers improved solutions for water treatment and pollution control by degrading organic pollutants and disinfecting water. Additionally, the energy efficiency of low-voltage plasma discharge, especially with alumina nanoparticles, can reduce industrial costs and environmental impact, making these technologies more appealing for widespread use. By integrating plasma with electrochemistry, we can utilize this system to accomplish various tasks. For example, this can be used to remove surface contamination and increase the surface

https://doi.org/10.1021/acsami.4c06007
ACS Appl. Mater. Interfaces 2024, 16, 33571−33577

energy of biomaterials in the ocean. The true potential of combining plasma with a catalyst surface lies in its ability to control reaction selectivity. For example, Tirumala et al. have used CuO_2 nanoparticles excited through a Mie resonance to drive hot electron-driven processes on a catalytic surface.[22,23] Our approach will, in principle, enable the implementation of this same general idea with plasma hot electrons and free radical species.

4. CONCLUSIONS

In conclusion, through the utilization of lithographically defined electrodes and metal/dielectric nanoparticles, which create a significant enhancement in the electric field, this study has achieved low voltage plasma discharge in aqueous solutions. By employing high voltage nanosecond pulse discharges, the research successfully generated transient plasma in liquid electrolytes at reduced applied voltages. Using gold and alumina nanoparticles reduces the threshold to generate plasma discharge to 17 and 14 kV, respectively. Furthermore, the plasma discharge intensity shows a significant (around 15×) enhancement with alumina particles at the same generation voltage compared to DI water without nanoparticles. The innovative approach of electric field enhancement has enabled the exploration of plasma discharge in water, overcoming the challenges associated with its high dielectric strength.

■ ASSOCIATED CONTENT

Supporting Information

The Supporting Information is available free of charge at https://pubs.acs.org/doi/10.1021/acsami.4c06007.

Explanation for choosing gold as an electrode material, raw data sets, and how the intensity-time traces are analyzed (PDF)

■ AUTHOR INFORMATION

Corresponding Author

Stephen B. Cronin − *Mork Family Department of Chemical Engineering and Materials Science and Department of Physics and Astronomy, University of Southern California, Los Angeles, California 90089, United States;* orcid.org/0000-0001-9153-7687; Email: scronin@usc.edu

Authors

Ruoxi Li − *Mork Family Department of Chemical Engineering and Materials Science, University of Southern California, Los Angeles, California 90089, United States;* orcid.org/0000-0002-6432-6072

Indu Aravind − *Department of Physics and Astronomy, University of Southern California, Los Angeles, California 90089, United States;* orcid.org/0000-0002-0908-9887

Sizhe Weng − *Ming Hsieh Department of Electrical Engineering, University of Southern California, Los Angeles, California 90089, United States;* orcid.org/0000-0002-6555-2442

Zhi Cai − *Mork Family Department of Chemical Engineering and Materials Science, University of Southern California, Los Angeles, California 90089, United States;* orcid.org/0000-0002-3741-5715

Boxin Zhang − *Mork Family Department of Chemical Engineering and Materials Science, University of Southern California, Los Angeles, California 90089, United States*

Complete contact information is available at: https://pubs.acs.org/10.1021/acsami.4c06007

Notes

The authors declare no competing financial interest.

■ ACKNOWLEDGMENTS

This research was supported by the Army Research Office (ARO) award no. W911NF2210284 (R.L.), National Science Foundation (NSF) award no. CBET-2112898 (I.A.), ECCS-2204667 (S.W.), and CHE-1954834 (B.Z.).

■ REFERENCES

(1) Li, J.; Ma, C.; Zhu, S.; Yu, F.; Dai, B.; Yang, D. A review of recent advances of dielectric barrier discharge plasma in catalysis. *Nanomaterials* **2019**, *9* (10), 1428.

(2) Snoeckx, R.; Bogaerts, A. Plasma technology-a novel solution for CO_2 conversion? *Chem. Soc. Rev.* **2017**, *46* (19), 5805−5863.

(3) Boutonnet Kizling, M.; Järås, S. G. A review of the use of plasma techniques in catalyst preparation and catalytic reactions. *Appl. Catal., A* **1996**, *147* (1), 1−21.

(4) Liu, C.-j.; Vissokov, G. P.; Jang, B. W.-L. Catalyst preparation using plasma technologies. *Catal. Today* **2002**, *72* (3−4), 173−184.

(5) Yang, S.; Aravind, I.; Zhang, B.; Weng, S.; Zhao, B.; Thomas, M.; Umstattd, R.; Singleton, D.; Sanders, J.; Cronin, S. B. Plasma-enhanced electrostatic precipitation of diesel exhaust using high voltage nanosecond pulse discharge. *J. Environ. Chem. Eng.* **2021**, *9* (6), 106565.

(6) Zhang, B.; Aravind, I.; Yang, S.; Weng, S.; Zhao, B.; Schroeder, C.; Schroeder, W.; Thomas, M.; Umstattd, R.; Singleton, D.; et al. Plasma-enhanced electrostatic precipitation of diesel exhaust particulates using nanosecond high voltage pulse discharge for mobile source emission control. *Sci. Total Environ.* **2022**, *851*, 158181.

(7) Gao, X.; Liang, J.; Wu, L.; Wu, L.; Kawi, S. Dielectric barrier discharge plasma-assisted catalytic CO_2 hydrogenation: synergy of catalyst and plasma. *Catalysts* **2022**, *12* (1), 66.

(8) Neuroth, C.; Mujahid, Z. u. i.; Berger, B.; Oberste-Beulmann, C.; Oppotsch, T.; Zhang, Q. Z.; Muhler, M.; Mussenbrock, T.; Korolov, I.; Schulze, J. The effects of catalyst conductivity and loading of dielectric surface structures on plasma dynamics in patterned dielectric barrier discharges. *Plasma Sources Sci. Technol.* **2023**, *32* (10), 105019.

(9) Zhang, Y.-R.; Neyts, E. C.; Bogaerts, A. Influence of the material dielectric constant on plasma generation inside catalyst pores. *J. Phys. Chem. C* **2016**, *120* (45), 25923−25934.

(10) Dobrynin, D.; Seepersad, Y.; Pekker, M.; Shneider, M. N.; Friedman, G.; Fridman, A. Non-equilibrium nanosecond-pulsed plasma generation in the liquid phase (water, PDMS) without bubbles: Fast imaging, spectroscopy and leader-type model. *J. Phys. D: Appl. Phys.* **2013**, *46*, 105201.

(11) Seepersad, Y.; Pekker, M.; Shneider, M. N.; Dobrynin, D.; Fridman, A. On the electrostrictive mechanism of nanosecond-pulsed breakdown in liquid phase. *J. Phys. D: Appl. Phys.* **2013**, *46* (16), 162001.

(12) Seepersad, Y.; Fridman, A.; Dobrynin, D. Anode initiated impulse breakdown in water: the dependence on pulse rise time for nanosecond and sub-nanosecond pulses and initiation mechanism based on electrostriction. *J. Phys. D: Appl. Phys.* **2015**, *48* (42), 424012.

(13) Seepersad, Y.; Pekker, M.; Shneider, M. N.; Fridman, A.; Dobrynin, D. Investigation of positive and negative modes of nanosecond pulsed discharge in water and electrostriction model of initiation. *J. Phys. D: Appl. Phys.* **2013**, *46* (35), 355201.

(14) Fujita, H.; Kanazawa, S.; Ohtani, K.; Komiya, A.; Kaneko, T.; Sato, T. Role of continuous discharge current for secondary streamer in water. *Int. J. Plasma Environ. Sci. Technol.* **2016**, *10* (1), 16−19.

(15) Sato, T. Lab Website. https://www.ifs.tohoku.ac.jp/bionano/research_eng.html (accessed on May 22, 2024).

(16) Pekker, M.; Seepersad, Y.; Shneider, M. N.; Fridman, A.; Dobrynin, D. Initiation stage of nanosecond breakdown in liquid. *J. Phys. D: Appl. Phys.* **2014**, *47* (2), 025502.

(17) Yang, S.; Zhao, B.; Aravind, I. A.; Wang, Y.; Zhang, B.; Weng, S.; Cai, Z.; Li, R.; Baygi, A. Z.; Smith, A.; et al. CO_2 Reduction to Higher

Hydrocarbons by Plasma Discharge in Carbonated Water. *ACS Energy Lett.* **2021**, *6* (11), 3924−3930.
(18) Chernets, N.; Dobrynin, D.; Ercan, U.; Joshi, S.; Ji, H.-F.; Brooks, A.; Fridman, G.; Cho, Y.; Fridman, A.; Friedman, G. Non-equilibrium plasma treatment of liquids, formation of plasma acid. In *Proceedings of the ISPC-20:20th International Symposium on Plasma Chemistry*; ISPC, 2011.
(19) Dobrynin, D.; Fridman, A.; Starikovskiy, A. Y. Reactive Oxygen and Nitrogen Species Production and Delivery Into Liquid Media by Microsecond Thermal Spark-Discharge Plasma Jet. *IEEE Trans. Plasma Sci.* **2012**, *40* (9), 2163−2171.
(20) Zhao, B.; Aravind, I.; Yang, S.; Cai, Z.; Wang, Y.; Li, R.; Subramanian, S.; Ford, P.; Singleton, D. R.; Gundersen, M. A.; et al. Nanoparticle-Enhanced Plasma Discharge Using Nanosecond High-Voltage Pulses. *J. Phys. Chem. C* **2020**, *124* (13), 7487−7491.
(21) Zhao, B.; Aravind, I.; Yang, S.; Wang, Y.; Li, R.; Cronin, S. B. Au Nanoparticle Enhancement of Plasma-Driven Methane Conversion into Higher Order Hydrocarbons via Hot Electrons. *ACS Appl. Nano Mater.* **2020**, *3* (12), 12388−12393.
(22) Tirumala, R. T. A.; Khatri, N.; Ramakrishnan, S. B.; Mohammadparast, F.; Khan, M. T.; Tan, S.; Wagle, P.; Puri, S.; McIlroy, D. N.; Kalkan, A. K.; et al. Tuning Catalytic Activity and Selectivity in Photocatalysis on Mie-Resonant Cuprous Oxide Particles: Distinguishing Electromagnetic Field Enhancement Effect from the Heating Effect. *ACS Sustainable Chem. Eng.* **2023**, *11* (44), 15931−15940.
(23) Tirumala, R. T. A.; Ramakrishnan, S. B.; Mohammadparast, F.; Khatri, N.; Arumugam, S. M.; Tan, S.; Kalkan, A. K.; Andiappan, M. Structure-property-performance relationships of dielectric Cu2O nanoparticles for Mie resonance-enhanced dye sensitization. *ACS Appl. Nano Mater.* **2022**, *5* (5), 6699−6707.

https://doi.org/10.1021/acsami.4c06007
ACS Appl. Mater. Interfaces 2024, 16, 33571−33577